Comparison of Isotropy Estimators for the Analysis of Reverberation Rooms

Marco Berzborn, Melanie Nolan, Efren Fernandez-Grande, Michael Vorländer

COMPARISON OF ISOTROPY ESTIMATORS FOR THE ANALYSIS OF REVERBERATION ROOMS

Marco Berzborn[1] **Mélanie Nolan**[2,3] **Efren Fernandez-Grande**[2] **Michael Vorländer**[1]
[1] Institute of Technical Acoustics, RWTH Aachen University, 52074 Germany
[2] Acoustic Technology, Department of Electrical Engineering, DTU, 2800 Denmark
[3] Saint-Gobain Ecophon, 265 75 Sweden
marco.berzborn@akustik.rwth-aachen.de

ABSTRACT

Reverberation-room measurements of absorption coefficients are subject to high uncertainties and irreproducibility across different laboratories. One reason is the lack of a sufficiently isotropic sound field both in steady-state and during the sound field decay. Recently, two different methods - based on the decomposition of the sound field into plane waves - have been proposed for the estimation and analysis of the sound field isotropy in reverberation rooms [1]–[5]. This study compares the two methods based on numerically calculated plane wave sound fields as well as experimental results obtained from array measurements in a reverberation room in different configurations. The room configurations comprise the room occupied with an absorber sample, with and without hanging panel diffusers, and additionally the empty room without diffusers. Both methods are compared regarding their suitability in the analysis of reverberation rooms and the required angular resolution for the plane wave decomposition.

1. INTRODUCTION

The random-incidence absorption coefficient is the parameter most used in architectural design and room acoustic simulations to specify the absorption performance of materials. It is measured in a reverberation chamber based on Sabine's formulations, for which a completely diffuse sound field must be established. A diffuse sound field is defined as requiring the average energy density to have minimal variation throughout space, and the energy to be propagating evenly in all directions (i.e., the sound field must be completely homogeneous and isotropic). Such condition cannot be achieved in a conventional room nor in a standardized reverberation chamber [6]. As the sound field found in one chamber differs from that found in a different chamber, the measured absorption coefficients can vary greatly from chamber to chamber. This results in difficulties with measurement reproducibility [7]. Yet, a standardized and accurate measure for the characterization of reverberation chambers is still lacking [8].

Numerous methods have been proposed for evaluating sound field diffusion or isotropy in reverberant environments [9]. One possible way of testing the isotropy of the sound field in a given chamber consists in measuring the directional distribution of sound energy, the idea being that, in a perfectly isotopic sound field, an equal amount of energy is observed for every direction [10]. The approach has shown particular promise in recent years, as technical developments in sensing methods have provided new possibilities for the analysis of spatial properties of sound fields.

In Refs. [1] and [2], Gover et al. proposed using a spherical microphone array to measure directional impulse responses in all directions. The squared impulse responses were integrated over a time period, enabling to compute and analyze the energy arriving from each direction over that time period, as well as the rate of the energy decay. In particular, the angular distribution of incident sound energy could be quantified by computing the directional diffusion index defined in Ref. [10]. By integrating over the full impulse response, or over successive restricted time ranges, the framework enables the analysis of isotropy in steady-state or as a function of time, respectively [2]. More recently, Berzborn et al. [3], [4] proposed to calculate the directional diffusion index based on directional energy decay curves (DEDCs) directly, as an alternative way of analyzing sound field isotropy over time. Another possible approach is to analyze directly the symmetry of the sound field to quantify isotropy. Nolan et al. [5] proposed to analyze the angular (wavenumber) spectrum; i.e., the directions from which plane waves arrive at the measurement points. The analysis is based on evaluating the proportion of isotropic energy in the sound field – energy that is rotationally symmetric – compared to the total energy energy in the sound field. This is achieved by expanding the angular spectrum of the sound field into spherical harmonics and evaluating the ratio of energy in the zeroth order (isotropic) over the total energy, that is isotropic and directional components. The methodology makes it possible to analyze isotropy both in steady state [5] and as a function of time [11], by processing the spatio-temporal data in a similar fashion as in Ref. [2].

This contribution aims at comparing the isotropy estimators proposed by Gover [2] and Nolan [5] for steady-state and decaying sound fields based on the DEDCs framework proposed in Ref. [4]. For this purpose the calculation of DEDCs is extended into a representation in the spherical harmonic domain, allowing for the direct calculation of the isotropy estimator proposed by Nolan [5].

The paper is organized as follows: Section 2 introduces the decomposition of a sound field into plane waves and the subsequent calculation of DEDCs. Section 3 introduces both isotropy estimation methods. Section 4 outlines the results of both estimation methods for a numeric simulation study, as well as an experimental investigation performed in a reverberation room.

2. DIRECTIONAL ENERGY DECAY CURVE ANALYSIS

Spherical microphone arrays (SMAs) – or microphone arrays in general – allow for the capture of directional room impulse responses (DRIRs) retaining directional information about the sound field in the room [12] and, therefore, prove to be a viable tool in the analysis of sound field isotropy [2], [5].

2.1 Plane Wave Decomposition with Spherical Arrays

A DRIR measured with an SMA can be written as a vector of L microphone signals

$$\mathbf{p}(k) = \left[p(k, r_1, \theta_1, \phi_1), \ldots, p(k, r_l, \theta_L, \phi_L)\right]^{\mathrm{T}}, \quad (1)$$

where r_l, θ_l, and ϕ_l are the radius, and the elevation and azimuth angles of the l'th sensor position, respectively, k is the wave number, and $(.)^{\mathrm{T}}$ denotes the transpose operator. For a plane wave sound field we may write the sound pressure at the microphone positions of an SMA as [12]

$$\mathbf{p}(k) = \mathbf{B}(k)\mathbf{a_{nm}}(k), \quad (2)$$

where the matrix $\mathbf{B}(k)$ contains the spherical harmonic (SH) basis functions$Y_n^m(\theta_l, \phi_l)$ of order n and degree m evaluated at the elevation and azimuth angles, as well as the modal strength function for the open sphere, both with a maximum SH order N. The vector $\mathbf{a_{nm}}(\mathbf{k})$ contains the SH coefficients defining the amplitude density function of the plane waves composing the sound field. For a single incident plane wave this becomes a vector containing the SH basis functions evaluated at the direction of arrival (DOA). Solving Eq. (2) for the spatial domain plane wave density function $\mathbf{a}(k)$ we decompose the sound field into a continuum of Q plane waves [12]

$$\mathbf{a}(k) = \frac{4\pi}{(N+1)^2}\mathbf{Y}^{\mathrm{T}}\mathbf{B}^{\dagger}(k)\mathbf{p}(k), \quad (3)$$

where the $(.)^{\dagger}$ operator denotes the Moore-Penrose Pseudo-inverse and

$$\mathbf{Y} = \left[\mathbf{y}^{\mathrm{T}}(\theta_1, \phi_1), \ldots, \mathbf{y}^{\mathrm{T}}(\theta_Q, \phi_Q)\right], \quad (4)$$

is the steering matrix of the array containing vectors of the SH basis functions evaluated at the q'th steering direction

$$\mathbf{y}(\theta_q, \phi_q) = \left[Y_0^0(\theta_q, \phi_q), \ldots, Y_N^N(\theta_q, \phi_q)\right]. \quad (5)$$

Applying the inverse discrete Fourier transform we calculate the time domain plane wave amplitude density $\mathbf{a}(t)$ which is to be interpreted as the angular distribution of plane waves impinging on the receiver over time.

2.2 Directional Energy Decay Curves

In [3], [4] the authors proposed DEDCs as a framework for the analysis of the energy distribution during the decay process of the sound field. For each time instance it enables the analysis of the remaining energy in the sound field with respect to the angular distributions and thus provides information about directions with dominant residual energy incidence.
The DEDC is calculated as the Schroeder integral [13] of the amplitude density function vector from Eq. (3), yielding the DEDCs for every steering direction

$$\mathbf{d}(t) = \int_t^{\infty} |\mathbf{a}(\tau)|^2 d\tau \quad = \mathbf{e_s} - \int_0^t |\mathbf{a}(\tau)|^2 d\tau, \quad (6)$$

where $\mathbf{e_s}$ is a vector containing the steady state energy for every steering direction.
We may also define the spherical harmonic directional energy decay curve (SH-DEDC) as the inverse SH transform of the DEDCs

$$\mathbf{d_{nm}}(t) = \mathbf{Y}^{\dagger}\mathbf{d}(t), \quad (7)$$

where $\mathbf{Y}^{\dagger}$ is the Moore-Penrose Pseudo-inverse of the SH basis matrix from Eq. (3), yielding the set of SH coefficients

$$\mathbf{d_{nm}}(t) = \left[d_{00}(t), d_{1(-1)}(t), \ldots, d_{NN}(t)\right]^{\mathrm{T}}. \quad (8)$$

The formulation in the SH domain allows for compressing the two-dimensional angular information over time to a one-dimensional set of linearly indexed spherical Fourier coefficients over time.

3. ISOTROPY ESTIMATION

3.1 Directional Energy Variation

Thiele [10] and Gover [2] proposed to estimate the sound field isotropy – they refer to it as directional diffusion – based on the mean of absolute directional differences of the energy incidence. We adapt the proposed method to the DEDC to analyze the directional variation of the sound field during the decay process. The directional variation is calculated as

$$\sigma_d(t) = \frac{1}{\langle d(t)\rangle_{\Omega}} \sum_{q=1}^{Q} |d(t, \theta_q, \phi_q) - \langle d(t)\rangle_{\Omega}|, \quad (9)$$

where $\langle d(t)\rangle_{\Omega}$ is the directional average of the DEDC evaluated for Q discrete directions spanning the entire spherical domain $\Omega = (\theta, \phi)$ at time instance t. For $(t = 0)$ this equals the variation of the sound field in steady-state. For compensation of the beamformer directivity pattern we normalize by the variation for the case of a single incident plane wave, here referred to as $\sigma_{e,0}$ [2]. Re-normalization by subtracting from one, yields the estimated isotropy of the sound field,

$$\mu_d(t) = 1 - \frac{\sigma_d(t)}{\sigma_{e,0}}. \quad (10)$$

Equation (10) is a function in the interval $\mu_d(t) \in [0, 1]$, which will be zero for a single incident plane wave and one for a perfectly isotropic sound field.
In the following we will refer to the method as the directional energy variation (DEV) estimator.

3.2 Monopole Ratio

In Ref. [5] Nolan proposed an isotropy estimator based on the weights of the SH coefficients of the magnitude wave number spectrum relative to their monopole moment. The estimator applied on the SH-DEDC can be written as [5],

$$\imath(t) = \frac{\sqrt{|d_{00}(t)|}}{\sum_{n=0}^{N} \sum_{m=-n}^{n} \sqrt{|d_{nm}(t)|}}, \qquad (11)$$

where the $d_{nm}(t)$ is the SH-DEDC detailed in Fig. 5 with it's respective monopole moment $d_{00}(t)$. Note that in contrast to [5] we apply the estimator to a function representing the squared magnitude, cf. Eq. (6), requiring an additional square root.
For an isotropic sound field it is assumed that the energy distribution is uniform over all angles of incidence and can consequently be represented by the zeroth-order SH coefficient – or the monopole moment – alone, yielding the maximum value of one for the isotropy estimation. For a single plane wave the sound field, the coefficients equal the SH basis function evaluated for the DOA, constituting almost no energy in the monopole coefficient, hence yielding an isotropy estimate of approximately zero. Note that, in contrast to the DEV estimator, a compensation for the beamformer directivity is not included in this approach.
In the following the estimator will be referred to as monopole ratio (MPR) estimator.

4. RESULTS

The isotropy estimators presented in Section 3 were compared based on numerical simulations using the analytic formulation for a plane wave incidence (cf. Eq. (2)) and experimental results obtained in a reverberation room.
For both studies an open dual-layer spherical microphone array – with radii $r = (0.25\,\mathrm{m}, 0.45\,\mathrm{m})$ – was chosen, each layer consisting of 144 sampling positions according to an equal-area distribution on the sphere [14]. Eleven additional sampling positions inside the volume of each sphere were used to achieve good stabilization of the eigenfrequencies of the spheres up to $kr = 9$ [15]. Using a SH order $N = 5$ this yields a usable frequency range of approximately $200\,\mathrm{Hz}$ - $3\,\mathrm{kHz}$ when fully equalizing for the modal strength of the array and thus ensuring a constant angular resolution [12]. All results presented in this paper are band-pass filtered to the $500\,\mathrm{Hz}$ third-octave frequency band. The plane wave decomposition was performed for 1000 uniformly distributed steering directions chosen by solving the Thomson problem [16], calculated using the approach by Thomas [17].

4.1 Numerical Study

The analytic solution for a plane wave incidence on a spherical microphone array (cf. Eq. (2)) was used to analyze the sensitivity of the estimators to the steady state energy distributions of different wave fields. The plane wave density function was calculated as

$$a_{nm}(k) = \sum_j S_j \mathrm{e}^{-i\varphi_j} Y_n^m(\theta_j, \phi_j), \qquad (12)$$

where (θ_j, ϕ_j) are the angles of incidence and S_j and φ_j are the amplitude and the phase of the signal carried by the j'th plane wave, respectively. All plane waves were simulated with a length of 16384 samples with randomly chosen phase angles and equal amplitudes. White noise with a signal-to-noise ratio of $60\,\mathrm{dB}$ was added to the microphone signals before performing the decomposition. Five different plane wave sound fields were considered: A single plane wave sound field S_0, a sound field S_1 inspired by the axial modes in the xy-plane in a rectangular room, two sound fields comprising 50 and 100 plane waves evenly distributed over the upper hemisphere (S_2) and the full sphere (S_3), respectively; sound field S_4 represents a combination of sound fields S_1 and S_3, where the energy of the waves in axial directions was increased by $6\,\mathrm{dB}$ compared to all other directions. Figure 2 shows the resulting steady state energy distributions normalized by their mean over all respective directions. The DOAs of the simulated waves are indicated by markers.
It is evident that for the sound fields S_0 and S_1 large variations in energy are observable not only in the directions of incidence but over the entire spherical domain, due to the limited angular resolution and imperfect stop-band attenuation of the plane wave decomposition beamformer. Clearly, S_0 represents an entirely anisotropic sound field. Sound field S_2 shows a uniform incidence of energy over the upper hemisphere, however, it can be observed that energy leaks into the lower hemisphere due to the side-lobes of the beamformer. Finally, sound field S_3 results in a almost uniform distribution of energy over the entire sphere with variations of less than $\pm 0.5\,\mathrm{dB}$ Note that even for a number of waves much larger than 100 slight variations in the estimated plane wave density persist due to finite angular resolution and the side-lobes of the plane wave decomposition beamformer.
Figure 1 and Table 1 show the estimated isotropy of the simulated sound fields. It is observed that the DEV estimator yields an isotropy value of approximately zero for sound field S_0, as expected from theory, whereas the MPR estimator results in a value of $\imath = 0.15$, reflecting the fluctuations seen in Fig. 2. This is due to spread of energy into the side-lobes of the beamformer, and as such is not caused by the estimator, but the beamformer response, which is not compensated for in the MPR estimator. Nolan [5] showed that for a perfect estimation of the wavenumber spectrum, a estimate of zero is achieved and further suggested solving the plane wave decomposition using ℓ_1-norm minimization for improved side-lobe attenuation and improved angular resolution when the solution

is sufficiently sparse, which however is not always known a priori. A similar behavior is observed for the sound fields S_1, which again is comprised of a small number of waves. For sound field S_3 the estimators yield a value of approximately 0.52 and 0.57. Finally, both estimators indicate an almost isotropic energy incidence for sound field S_3. It has to be noted that a sound field with 40 or more waves with uniform DOAs (not plotted for brevity) already resulted in an DEV isotropy estimate $\mu > 0.95$ whereas the MPR estimator required a larger number of waves for the same isotropy value, indicating a higher sensitivity – for changes in sound fields comprising a large number of waves – before it saturates. This is also evident from the results obtained for sound field S_4, where the MPR estimator indicates a larger reduction in isotropy than the DEV estimator. In summary MPR led to higher values of isotropy for few incident waves, but showed a more sensitive response in sound fields with a large number of waves.

	S_0	S_1	S_2	S_3	S_4
DEV	0.0	0.2	0.52	0.99	0.89
MPR	0.15	0.39	0.57	0.95	0.8

Table 1. Estimated isotropy for the numerically simulated steady-state plane wave sound fields from Fig. 2.

4.2 Experimental Study

The DEDCs were analyzed experimentally for a rectangular reverberation room at the Technical University of Denmark (2800 Kgs. Lyngby, Denmark) in three configurations [1]: The empty room without panel diffusers and the room with and without panel diffusers, but occupied with an absorbing sample of glass wool. The glass wool has a surface area of $10.8\,\mathrm{m}^2$ and an absorption coefficient of 1.04 – measured according to ISO-354:2003 [18] – for the $500\,\mathrm{Hz}$ third-octave band. The dimensions of the room

[1] For a more detailed, but separate discussion of the results presented in this subsection, the reader is referred to Refs. [4] and [11]

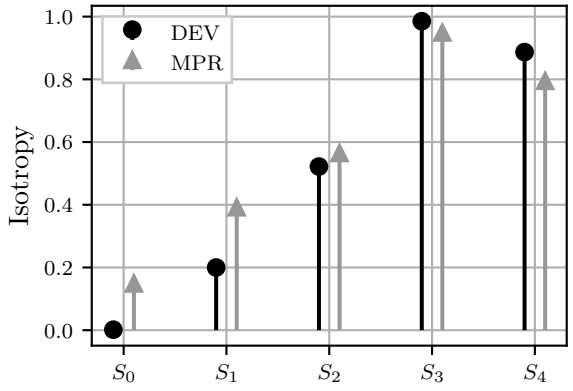

Figure 1. Estimated isotropy for the numerically simulated steady-state plane wave sound fields from Fig. 2.

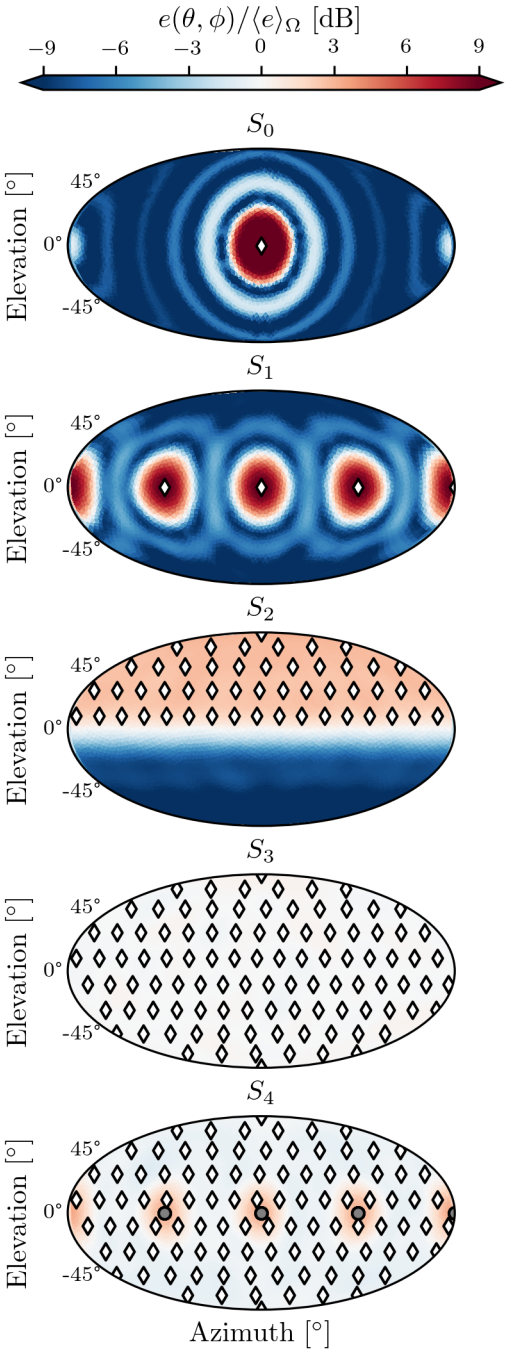

Figure 2. Normalized steady-state energy distributions resulting from numerically simulated plane waves with random phases. Diamonds mark the DOAs of the respective plane waves constituting the sound field. The round markers in S_4 represent waves with amplitudes increased by $6\,\mathrm{dB}$ over waves marked with diamonds. All grid-lines represent steps of $45°$

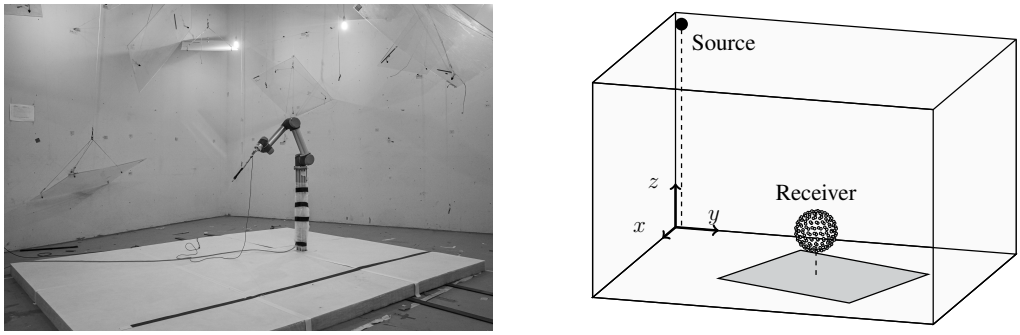

(a) (b)

Figure 3. The experimental setup with source and receiver positions as well as the absorber position in the reverberation room. The pose of the robotic arm in Fig. 3(a) marks the south pole of the inner sphere. For better visual interpretability only sampling positions on the outer sphere are shown in Fig. 3(b).

are $(x, y, z) = (6.25\,\mathrm{m}, 7.85\,\mathrm{m}, 4.9\,\mathrm{m})$ with an approximate volume of $245\,\mathrm{m}^3$ and a Schroeder frequency slightly over $300\,\mathrm{Hz}$. Figure 3 details the experimental setup of the room including the absorber sample. The sound field in the room was excited by a source mounted in the corner below the ceiling at approximately $(0.2\,\mathrm{m}, 0.2\,\mathrm{m}, 4.7\,\mathrm{m})$, cf. Fig. 3. A UR5 (Universal Robots, Odense, Denmark) scanning robot arm in combination with a pressure-field $1/2''$ Brüel & Kjær type 4192 microphone was used to sequentially sample the dual-layer spherical array centered at $(2.98\,\mathrm{m}, 4.16\,\mathrm{m}, 1\,\mathrm{m})$, cf. Fig. 3. Impulse response measurements were performed with the ITA-Toolbox [19] using exponential sweeps as excitation signal for each sampling position. The measurement duration for a full sequential array ranged from $2.5\,\mathrm{h}$ for the occupied room to $4.5\,\mathrm{h}$ for the empty room. Temperature changes remained below $0.3°$ during the sequential measurement of the full array.

The DEDCs were calculated by evaluating the Schroeder integral in Eq. (6) up to the intersection time with the noise floor, cf. Method B in [20]. The DEDCs were finally truncated at the times corresponding to a level of $20\,\mathrm{dB}$ above the noise floor to compensate for errors introduced by limiting the integration interval [21]. The chosen method does not impose any constraints on the linearity of the logarithmic decay function, and therefore is suitable when dealing with multi-exponential decay curves expected in this specific experimental setup [4], [22]. The DEDCs were truncated once more to the shortest joint decay time corresponding to a decay of $35\,\mathrm{dB}$ ensuring decay curves with joint valid length.

Figure 4 shows the normalized energy incidence for four different time instances corresponding to the steady-state and decays of $-5\,\mathrm{dB}$, $-15\,\mathrm{dB}$, and $-25\,\mathrm{dB}$. The times were extracted from the omnidirectional decay curve, calculated from the zeroth-order SH coefficient. The contour plots are aligned with the coordinate-axes in Fig. 3.

It is evident that without panel diffusers the sound field shows a concentration of energy in the DOAs corresponding to the axial modes of the room. For the steady-state sound field in the empty room, maxima are found in the $\pm x$, $\pm y$ and $\pm z$-axes of the room, clearly indicating dominant axial modes. While the maxima are initially reduced at $t_{-5\mathrm{dB}}$, dominant floor reflections are observed during the later decay causing an increase of incident energy in the lower hemisphere relative to the mean. Similarly, strong maxima in the DEDCs are found at $\phi = (-90°, 0°, 90°, 180°)$ for the occupied room without diffuser panels. Initially the mixing of energy improves around $t_{-5\mathrm{dB}}$, followed again by a relative increase of incident energy for the axial and tangential modes in the xy-plane. This indicates dominant energy flows tangential to the absorber over time, caused by a slower decay rate of modes corresponding to waves at grazing incidence compared to oblique modes. The phenomenon is mitigated when the panel diffusers – redirecting sound waves into the absorber – are installed, yielding a more uniform distribution of energy over the upper hemisphere after $t_{-5\mathrm{dB}}$. A representation of the SH-DEDCs analogous to the contour plots in Fig. 4 is given in Fig. 5. Vertical lines indicate the times for which respective contour plots are shown in Fig. 4. It is evident that the energy flows tangential to the absorber found in the room configuration without panel diffusers result in an increase of energy in SH coefficients of higher orders. The increase of energy in the axial modes of the sound field over time is represented by an increase of energy in the coefficients of orders two to four after approximately $0.75\,\mathrm{s}$, indicating a more complex sound field with reduced symmetry.

From the bottom part of Fig. 4 it can be observed that both isotropy estimators qualitatively follow the same temporal trends, reflecting the temporal evolution of energy distributions as well as the corresponding systematic defects in the isotropy of the sound fields outlined above. Both estimators indicate an initial increase in isotropy followed by a steady decrease for the room configurations without panel diffusers. However, in all cases, the MPR estimator indicates a overall lower isotropy value and outlines more pronounced fluctuations over time, whereas the DEV estimator shows less variations over time. In the occupied room with panel diffusers, the MPR estimator indicates a maximum isotropy value of $\imath = 0.55$, reflecting the almost uniform distribution of energy over the upper hemisphere. The DEV estimator results in a maximum esti-

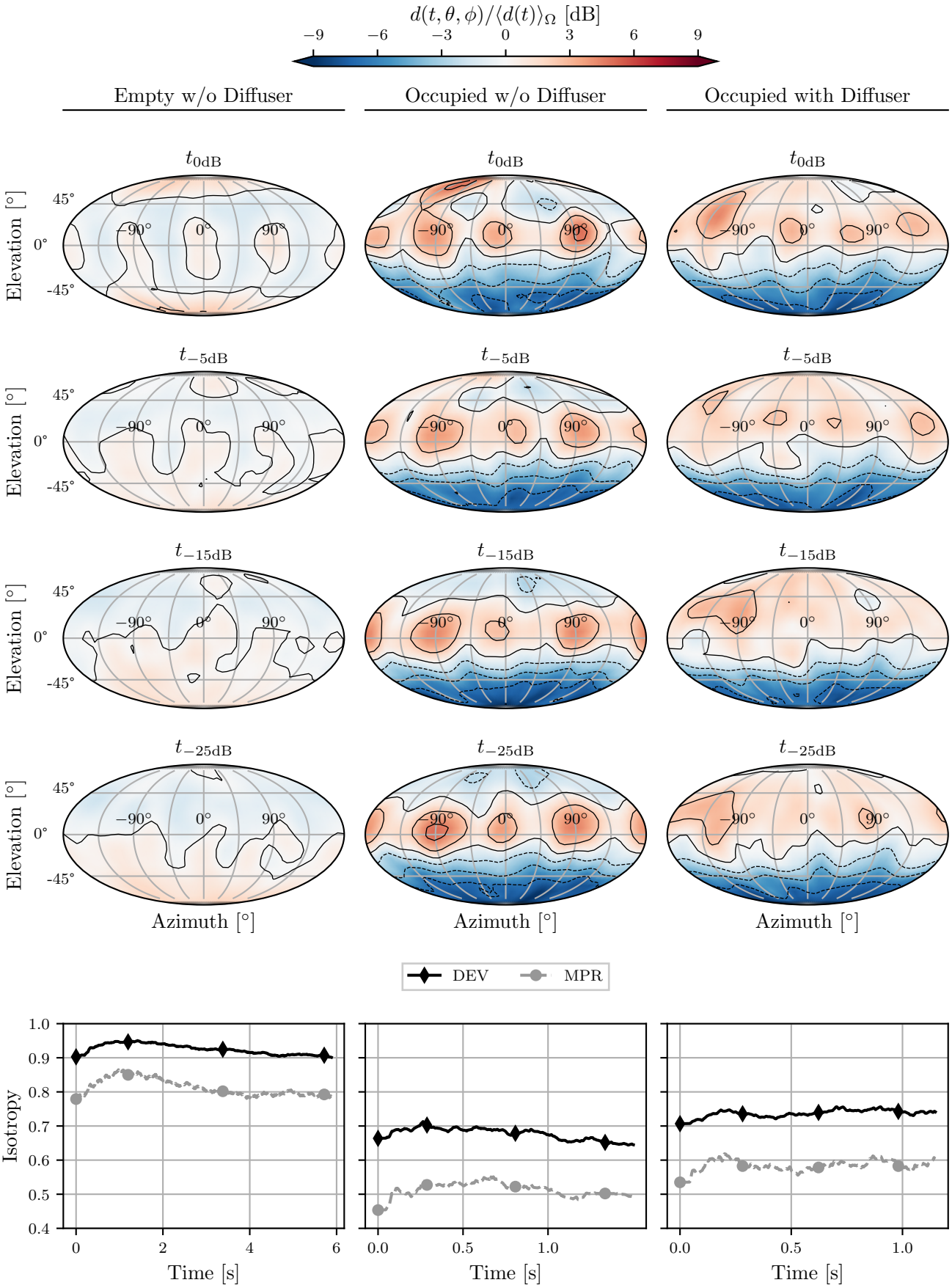

Figure 4. The DEDCs normalized by the mean over all directions of incidence (top) and estimated isotropy (bottom) for the 500 Hz third-octave frequency band. The contour lines are representative of levels marked in the color bar, dashed lines indicate negative contour levels. Markers in the isotopy plots correspond to the contour plots depicted above in the order from top to bottom.

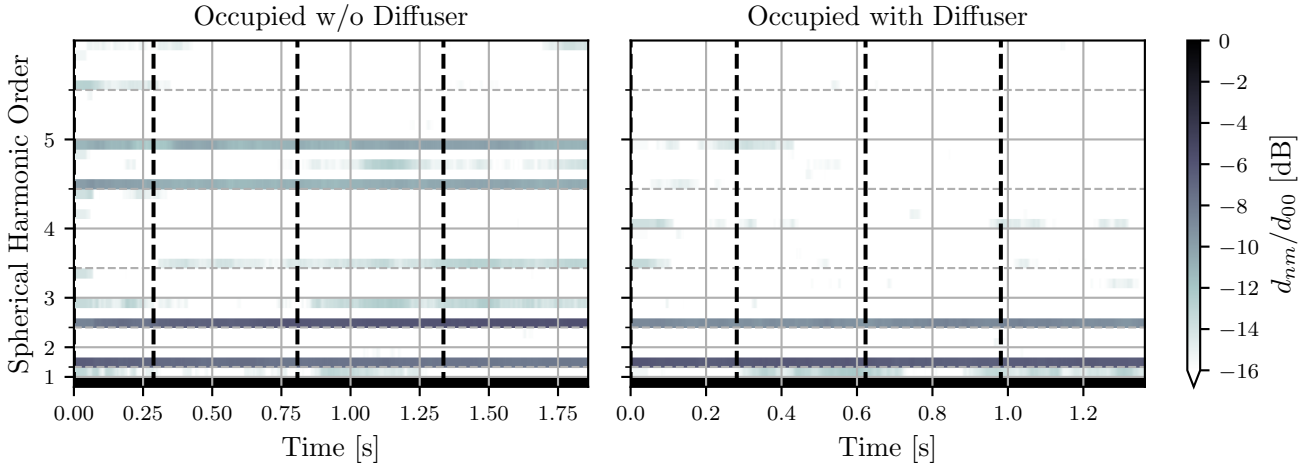

Figure 5. The SH-DEDCs normalized by their respective monopole moment for the 500 Hz third octave frequency band. The coefficients for the respective spherical harmonic order are plotted above the respective tick label. Dashed tick marks indicate degree zero of the corresponding order; vertical lines indicate times for which contour plots are shown in Fig. 4.

mate of $\mu_d = 0.75$, seemingly over-estimating the isotropy and neglecting the remaining apparent fluctuations. This is especially evident for the occupied room without diffuser panels, where a small number of waves dominate the energy distribution. The MPR estimator yields a maximum isotropy of $\imath = 0.52$ whereas, the DEV estimator indicates value of $\mu_d = 0.71$.

5. DISCUSSION

The used array geometry is expected to yield valid results in the frequency range from approximately 200 Hz - 3 kHz. The angular resolution and side-lobe attenuation is limited by the spherical harmonic order set during the decomposition of the sound field into a plane wave basis, and inevitably linked to the number of sensor positions available in the sequential array. Note that the resulting wave number spectrum may also be calculated in the spatial domain in a least-squares sense, allowing for arbitrary array geometries, but being subject to comparable limitations.

Both, the finite main-lobe resolution and side-lobe attenuation directly affect the accuracy of the isotropy estimation. The angular resolution primarily defines the number of waves resulting in a maximum isotropy estimation when considering a uniform distribution of the latter, and consequently saturating the estimator. The MPR estimator proves to require a larger number of incident waves to saturate in comparison to the DEV estimator. However, considering a small number of incident waves, the MPR yields a higher estimate than the DEV estimator. This is due to the angular variations of the beamformer directivity pattern, which – in contrast to the DEV estimator – is not compensated for. Nevertheless, the MPR estimator shows to be more sensitive to local fluctuations in incident energy when a large number of incident waves is present. This is evident from sound field S_4 in the numerical study, but especially prominent in the experimental study, where the DEV estimator seemingly overestimates the isotropy of the sound field in all room-configurations, showing a limited response to changes in isotropy. While the temporal change in the estimated isotropy qualitatively follows the same trend, a clear quantitative difference is observed.

6. CONCLUSIONS

In this paper we presented a comparison of two sound field isotropy estimators. Both estimators were compared based on a numerical study for a steady-state sound field, as well as on a experimental study of the steady state and decaying sound field conducted in a reverberation room in three different configurations, aiming at creating varying degrees of sound field diffuseness. The configurations included the empty reverberation room without panel diffusers and the room occupied with an absorbing sample on the floor and with and without panel diffusers installed from the ceiling. Results showed qualitatively comparable results for both estimators. This is especially evident for the temporal evolution of both estimators during their decay. However, quantitative differences were found in the simulation study as well as the experimental study. For a small number of incident waves, the MPR estimator estimated a higher isotropy value due to the lacking compensation of the beamformer response, while an overestimation in sound field isotropy was observed for the DEV estimator when a large number of incident waves was present. Hence, the MPR estimator may be more suited for the analysis of reverberation rooms, responding more sensibly to small changes in the isotropy of complex sound fields comprised of a large number of incident waves. It does however have to be noted, that this response is not necessarily linear and may include an additional bias introduced by the lacking equalization of the beamformer side-lobes introduced during the plane wave decomposition.

Even though, the time-dependent estimation of sound field isotropy is expected to be of value in the classification of reverberation rooms, it must still be recognized that it does not give sufficient information on the causes of a non-diffuse sound field. The additional analysis of the DEDC

is expected to give more insights into systematic defects in the isotropy of the sound field and the reason for the well known inconsistencies between laboratories used for measurements of the absorption coefficient.

7. ACKNOWLEDGEMENTS

The work presented here is jointly supported by the German Research Foundation (Grant No. DFG VO 600 41-1), the Innovation Fund Denmark (Grant No. 8054-00042B), and Saint-Gobain Ecophon.
The authors would like to thank Samuel A. Verburg for his assistance with the experimental setup.

8. REFERENCES

[1] B. N. Gover, J. G. Ryan, and M. R. Stinson, "Microphone array measurement system for analysis of directional and spatial variations of sound fields.," *J. Acoust. Soc. Am.*, vol. 112, no. 5, pp. 1980–1991, 2002.

[2] B. N. Gover, J. G. Ryan, and M. R. Stinson, "Measurements of directional properties of reverberant sound fields in rooms using a spherical microphone array," *J. Acoust. Soc. Am.*, vol. 116, no. 4, pp. 2138–2138, 2004.

[3] M. Berzborn and M. Vorländer, "Investigations on the Directional Energy Decay Curves in Reverberation Rooms," in *Proc. of Euronoise*, Hersonissos, 2018, pp. 2005–2010.

[4] M. Berzborn, M. Nolan, E. Fernandez-Grande, and M. Vorländer, "On the Directional Properties of Energy Decay Curves," in *Proceedings of the 23rd International Congress on Acoustics*, Aachen, Germany, 2019, pp. 4043–4050.

[5] M. Nolan, E. Fernandez-Grande, J. Brunskog, and C.-H. Jeong, "A wavenumber approach to quantifying the isotropy of the sound field in reverberant spaces," *J. Acoust. Soc. Am.*, vol. 143, no. 4, pp. 2514–2526, Apr. 2018.

[6] M. Nolan, S. A. Verburg, J. Brunskog, and E. Fernandez-Grande, "Experimental characterization of the sound field in a reverberation room," *J. Acoust. Soc. Am.*, vol. 145, no. 4, pp. 2237–2246, Apr. 2019.

[7] R. E. Halliwell, "Inter-laboratory variability of sound absorption measurement," *J. Acoust. Soc. Am.*, vol. 73, no. 3, pp. 880–886, Mar. 1983.

[8] D. T. Bradley, M. Mueller-Trapet, J. R. Adelgren, and M. Vorlaender, "Effect of boundary diffusers in a reverberation chamber: Standardized diffuse field quantifiers," *J. Acoust. Soc. Am.*, vol. 135, pp. 1898–1906, 2014.

[9] C.-H. Jeong, M. Nolan, and J. Balint, "Difficulties in comparing diffuse sound field measures and data/code sharing for future collaboration," in *Proc. of Euronoise*, Hersonissos, 2018, pp. 1997–2004.

[10] R. Thiele, "Richtungsverteilung und Zeitfolge der Schallrückwürfe in Räumen," *Acta Acust. United Ac.*, vol. 3, no. 4, pp. 291–302, 1953.

[11] M. Nolan, M. Berzborn, and E. Fernandez-Grande, "Isotropy in decaying reverberant sound fields," *J. Acoust. Soc. Am.*, vol. 148, no. 2, pp. 1077–1088, Aug. 2020.

[12] B. Rafaely, "The spherical-shell microphone array," *IEEE Transactions on Audio, Speech and Language Processing*, vol. 16, no. 4, pp. 740–747, 2008.

[13] M. R. Schroeder, "New Method of Measuring Reverberation Time," *J. Acoust. Soc. Am.*, vol. 37, no. 6, pp. 1187–1187, 1965.

[14] P. Leopardi, "A partition of the unit sphere into regions of equal area and small diameter," *Electron. T. Numer. Ana.*, vol. 25, no. 12, pp. 309–327, 2006.

[15] G. Chardon, W. Kreuzer, and M. Noisternig, "Design of spatial microphone arrays for sound field interpolation," *IEEE J. Sel. Topics Signal Process.*, vol. 9, no. 5, pp. 780–790, 2015.

[16] J. Thomson, "XXIV. On the structure of the atom: An investigation of the stability and periods of oscillation of a number of corpuscles arranged at equal intervals around the circumference of a circle," *Lond. Edinb. Dubl. Phil. Mag.*, vol. 7, no. 39, pp. 237–265, Mar. 1904.

[17] M. R. P. Thomas, "Fast computation of cubature formulae for the sphere," in *2017 Hands-Free Speech Communications and Microphone Arrays (HSCMA)*, San Francisco, CA, USA: IEEE, 2017, pp. 201–205.

[18] International Organization for Standardization, *ISO 354:2003 - Measurement of sound absorption in a reverberation room*, 2003.

[19] M. Berzborn, R. Bomhardt, J. Klein, J.-G. Richter, and M. Vorländer, "The ITA-Toolbox: An Open Source MATLAB Toolbox for Acoustic Measurements and Signal Processing," in *Proceedings of the 43rd Annual German Congress on Acoustics*, Kiel, 2017, pp. 222–225.

[20] M. Guski and M. Vorländer, "Comparison of Noise Compensation Methods for Room Acoustic Impulse Response Evaluations," *Acta Acust. United Ac.*, vol. 100, no. 2, pp. 320–327, Mar. 1, 2014.

[21] A. Lundeby, T. E. Vigran, H. Bietz, and M. Vorl, "Uncertainties of Measurements in Room Acoustics," *Acta Acust. United Ac.*, vol. 81, no. 4, pp. 344–355, Jul. 1, 1995.

[22] J. Balint, F. Muralter, M. Nolan, and C.-H. Jeong, "Bayesian decay time estimation in a reverberation chamber for absorption measurements," *J. Acoust. Soc. Am.*, vol. 146, no. 3, pp. 1641–1649, Sep. 2019.